

Doping Profile Engineered Triple Heterojunction TFETs With 12-nm Body Thickness

Chin-Yi Chen¹, Hsin-Ying Tseng², Hesameddin Ilatikhameneh³, Tarek A. Ameen⁴,
Gerhard Klimeck⁵, *Fellow, IEEE*, Mark J. Rodwell⁶, *Fellow, IEEE*, and Michael Povolotskyi⁷

Abstract—Triple heterojunction (THJ) tunneling field-effect transistors (TFETs) have been proposed to resolve the low ON-current challenge of TFETs. However, the design space for THJ-TFETs is limited by fabrication challenges with respect to device dimensions and material interfaces. This work shows that the original THJ-TFET design with 12-nm body thickness has poor performance because its subthreshold swing (SS) is 50 mV/decade and the ON-current is only 6 $\mu\text{A}/\mu\text{m}$. To improve the performance, the doping profile of THJ-TFET is engineered to boost the resonant tunneling efficiency. The proposed THJ-TFET design shows an SS of 40 mV/decade over four orders of drain current and an ON-current of 325 $\mu\text{A}/\mu\text{m}$ with $V_{GS} = 0.3$ V. Since THJ-TFETs have multiple quantum wells and material interfaces in the tunneling junction, quantum transport simulations in such devices are complicated. State-of-the-art mode-space quantum transport simulation, including the effect of thermalization and scattering, is employed in this work to optimize THJ-TFET design.

Index Terms—Atomistic mode-space quantum transport, channel thickness, scattering, triple heterojunction (THJ) tunneling field-effect transistors (TFETs).

I. INTRODUCTION

POWER consumption in CPUs has impacted Moore's law significantly [1], [2]. An obvious solution to reduce the power supply is to replace the metal-oxide-semiconductor field-effect transistors (MOSFETs), which is

Manuscript received March 20, 2021; accepted April 19, 2021. Date of publication May 6, 2021; date of current version May 21, 2021. This work was supported in part by the National Science Foundation Energy-Efficient Computing: from Devices to Architectures (E2CDA) Type I collaborative research on "A Fast 70mV Transistor Technology for Ultra-Low-Energy Computing" under Award 1639958; in part by the Semiconductor Research Corporation under Task ID 2694.003; in part by the U.S. National Science Foundation, for the use of nanoHUB.org computational resources operated by the Network for Computational Nanotechnology, under Grant EEC-1227110, Grant EEC-0228390, Grant EEC-0634750, Grant OCI-0438246, and Grant OCI-0721680; in part by an NSF Peta-Apps, for NEMO5 developments, under Award OCI-0749140; in part by Intel Corporation; and in part by the Extreme Science and Engineering Discovery Environment (XSEDE) at San Diego Supercomputer Center (SDSC) Dell Cluster with Intel Haswell Processors (Comet) through 50000.0 SUs under Grant TG-ECS190009. The review of this article was arranged by Editor N. Xu. (Corresponding author: Chin-Yi Chen.)

Chin-Yi Chen, Hesameddin Ilatikhameneh, Tarek A. Ameen, and Gerhard Klimeck are with the Department of Electrical and Computer Engineering, Purdue University, West Lafayette, IN 47907 USA (e-mail: r99941001@gmail.com).

Hsin-Ying Tseng and Mark J. Rodwell are with the Department of Electrical and Computer Engineering, University of California at Santa Barbara, Santa Barbara, CA 93016 USA.

Michael Povolotskyi is with Jacobs Corporation, Hanover, MD 21076 USA and also with Arizona State University, Tempe, AZ 85281 USA.

Color versions of one or more figures in this article are available at <https://doi.org/10.1109/TED.2021.3075190>.

Digital Object Identifier 10.1109/TED.2021.3075190

limited by the Boltzmann tyranny, with new devices such as the tunneling field-effect transistors (TFETs) [3]–[14] and negative-capacitance field-effect transistors (NC-FETs) [15], [16]. However, these steep subthreshold slope devices come with challenges that hinder their widespread applications. The primary challenge of TFETs is their low ON-current. TFETs are shown to suffer from low ON-current issue since the quantum tunneling probability is usually much lower than one [17]. The tunneling probability depends on several factors, such as tunneling distance, electric field, resonance conditions, and effective tunneling mass. Several approaches have been introduced to increase the tunneling probability based on optimizing these four factors. For example, in GaN-based heterojunction TFETs, the tunneling distance is reduced by engineering the band diagram [18]; in a dielectric engineered TFET, the electric field at the tunneling junction is increased by using two different dielectrics [19]; in a resonance-TFET, quantum resonances are used to increase the tunneling probability close to one [20]; in a phosphorene-based TFET, the low effective tunneling mass increases the tunneling probability [21].

A triple heterojunction (THJ-) TFET based on III–V materials allows an advantage in optimizing all of the factors mentioned above. A THJ reduces the tunneling distance using the band diagram engineering. It also uses resonance tunneling to improve the tunneling probability in the ON-state and provides small effective tunneling mass due to III–V materials [22]–[25].

Despite the benefits of THJ-TFETs, the fabrication constraints, such as device dimensions and material combinations, limit the performance of a THJ-TFET. For the III–V TFET, achieving a sub-5-nm body thickness is challenging and is yet to be demonstrated. We investigated the doping profile design to improve the performance without the necessity of such thin body thickness.

For example, a 4-nm-thick THJ-TFET with a conventional p-i-n doping profile shown in Fig. 1(a) predicts an excellent performance; however, as the body thickness (T_{ch}) approaches a realistic value of 12 nm, the performance degrades. The reason for the high sensitivity of performance on body thickness in the original design is that, in p-i-n structures, the electric field (E) at the tunnel junction depends on both the depletion width (W_D) and the scaling length (λ), as shown in the following equation [26], [27]:

$$E \propto 1/(W_D + \lambda(T_{ch})). \quad (1)$$

To address these issues in designing THJ-TFETs, the doping profile is engineered, as shown in Fig. 1(b). By replacing

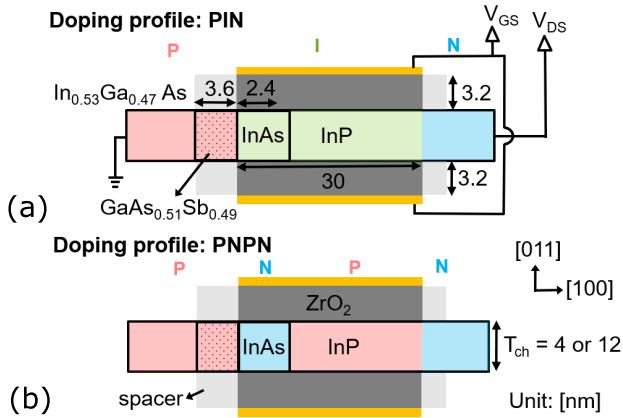


Fig. 1. Device design of a THJ TFET with (a) conventional doping profile (p-i-n) and (b) optimized doping profile (p-n-p-n).

the intrinsic part of the channel with the doped regions, the electric field is determined by the depletion width, which is not strongly dependent on T_{ch} , as shown in the following equation:

$$E \propto 1/(W_{D,source} + W_{D,channel}). \quad (2)$$

Hence, the proposed design provides better performance for thicker devices by reducing the impact of thickness on the electrostatic profile.

The proposed design also considers fabrication technology constraints, including the limitation of the doping density in each material, the width of the strained quantum well, the crystal growth direction, and the channel material's choice to have a high-quality oxide interface. The proposed design shows the subthreshold swing (SS) of 40 mV/decade over four orders of drain current. The high ON-current of 325 $\mu\text{A}/\mu\text{m}$ is achieved with a low supply voltage (V_{DD}) of 0.3 V.

The device design optimization is performed using the Nanoelectronics Modeling tool NEMO5 [28], [29]. The atomistic tight-binding method uses a ten orbital $sp^3d^5s^*$ basis, which is parameterized to hybrid functional (HSE06) calculations for varieties of strained systems [30]. Carrier transport in THJ-TFETs is complex due to the presence of quantum wells in the tunneling region. The nonequilibrium quantum mechanics of the system includes the electron–electron scattering and the electron–phonon scattering of carriers in these quantum wells, tunneling process at multiple interfaces, and quantum confinement effects [31]–[38].

Trap-assisted tunneling and thermalization in the quantum well are major issues that degrade TFET's OFF-state [39]–[44]. In this work, we use the state-of-the-art quantum transport method, including thermalization effects, to investigate the new design. Such a method has been developed and verified with experiments [45], [46]. The nonidealities are implicitly considered through a decaying parameter [46]. Since a real-space atomistic simulation is computationally challenging for devices with a large dimension, the atomistic mode-space approach developed in [47] is applied in this work.

This article is divided into four sections. The THJ-TFET device structure that satisfies fabrication constraints is presented in Section II. The design principles for the THJ-

TFET with a body thickness of 12 nm are discussed in Section III. In Section IV, we demonstrate the performance of the proposed THJ-TFET. The impact of the channel doping density is further discussed in Section V.

II. THJ-TFET DEVICE STRUCTURE

Fig. 1 shows the double-gated ultrathin-body (UTB) THJ-TFET studied in this work. Fig. 1(a) shows the THJ-TFET with a conventional p-i-n doping profile. It consists of a P-doped source, an intrinsic channel, and an N-doped drain. In the P-doped source, $\text{In}_{0.53}\text{Ga}_{0.47}\text{As}$ and $\text{GaAs}_{0.51}\text{Sb}_{0.49}$ have the doping density of $N_a = 5 \times 10^{19} \text{ cm}^{-3}$. InAs and InP channels are intrinsic. In the N-doped drain, InP has the doping density of $N_d = 2 \times 10^{19} \text{ cm}^{-3}$.

The UTB confinement direction is along $\langle 011 \rangle$ crystal direction, and the electron transport direction is along $\langle 100 \rangle$ crystal direction. The electron transport direction is the same as the crystal growth direction to simulate the device structure fabricated by the vertical Fin-TFET technology [48]. The choice of the materials in the heterojunction is compatible with current crystal growth technology limitations. The substrate is assumed to be InP such that InAs quantum well is under 3.41% biaxial compressive strain, while $\text{In}_{0.53}\text{Ga}_{0.47}\text{As}$ and $\text{GaAs}_{0.51}\text{Sb}_{0.49}$ are not strained since they are lattice-matched to InP substrate. The technologies of growing $\text{In}_{0.53}\text{Ga}_{0.47}\text{As}$, $\text{GaAs}_{0.51}\text{Sb}_{0.49}$, and InAs on InP(100) substrate through molecular beam epitaxy (MBE) are all well-developed [49]–[51].

The width of the $\text{GaAs}_{0.51}\text{Sb}_{0.49}$ source quantum well is 3.6 nm. The width of the strained InAs channel quantum well is 2.4 nm, which is less than the critical thickness of 4 nm [52], [53]. The choice of the InAs and GaAsSb quantum well widths is optimized based on fabrication constraints, and the alignment of InAs and GaAsSb quantum well confines states in the tunneling window. The gate length is 30 nm, and the oxide thickness is 3.2 nm. The oxide material is assumed to be ZrO_2 with a relative dielectric constant of 15. The source is grounded. The drain is under the applied supply voltage ($V_{DD} = 0.3 \text{ V}$). The source to drain bias (V_{DS}) is 0.3 V. The spacer is assumed to be air with a dielectric constant of 1 to reduce the fringing field's impact [54]. Drain-induced barrier tunneling (DIBT) may negatively affect performance if a higher dielectric constant material is used in the spacer [55].

Fig. 1(b) shows the proposed design with the same device structure, as shown in Fig. 1(a), while the doping is changed to the p-n-p-n doping profile. In the optimized p-n-p-n doping profile, the InAs channel quantum well is doped to N-type with $N_d = 5 \times 10^{19} \text{ cm}^{-3}$. The InP channel is doped to P-type with $N_a = 2 \times 10^{19} \text{ cm}^{-3}$. III–V UTB materials with such high doping density in the thin-film structure have been demonstrated and applied to the high electron mobility transistors (HEMT) and the heterojunction bipolar transistors (HBT) [56], [57]. The abrupt junction is assumed in this work, and no random dopant fluctuation is considered [58]–[61].

III. ORIGINAL THJ-TFET DESIGN PRINCIPLES

The design principle of the original THJ-TFETs is introduced in this section before describing the new design,

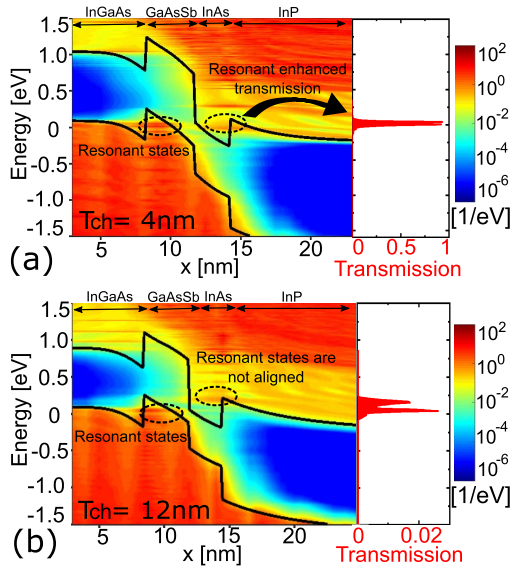


Fig. 2. Original THJ-TFET design principle: alignment of resonant states. (a) and (b) Energy-resolved LDOSs and transmission for 4- and 12-nm-thick THJ-TFETs when the device is operated in the ON-state.

p-n-p-n-doped THJ-TFET. The energy-resolved local density of states (LDOSs) and the transmission probability for the original THJ-TFET with different body thicknesses (T_{ch}) are shown in Fig. 2. The doping profile is a conventional p-i-n doping profile shown in Fig. 1(a). The LDOS in Fig. 2 is calculated when the device is operated in the ON-state, where the gate-to-source bias (V_{GS}) is 0.3 V. In Fig. 2(a), the alignment of the resonant states in the GaAsSb and InAs quantum wells results in the enhanced resonant tunneling such that the transmission probability is close to 1. The electrons tunnel from the P-InGaAs source, through the P-GaAsSb and N-InAs layers, into the N-InP channel. On the other hand, in Fig. 2(b), when the body thickness increases to 12 nm, the resonant states are not aligned due to the worse gate control. The transmission, therefore, reduces 1~2 orders compared to the case of 4-nm body thickness.

The key design rule of THJ-TFETs is to align the resonant states of two quantum wells in the tunneling junction and introduce the resonant enhanced transmission. In Section IV, the performance of 12-nm-thick THJ-TFET is improved by aligning the resonant states through the proposed p-n-p-n doping profile shown in Fig. 1(b).

IV. IMPROVED THJ-TFET WITH p-n-p-n DOPING PROFILE

In this section, the performance of THJ-TFET with the p-n-p-n doping profile is demonstrated. The p-n-p-n doping profile was originally proposed for homojunction TFETs to improve electric field in the tunneling region [62]–[65]. It plays a more significant role in THJ-TFETs with thick-body thickness. The p-n-p-n doping profile can be engineered in THJ-TFETs not only to increase the electric field but also to help to align the resonant states that introduce the resonance tunneling.

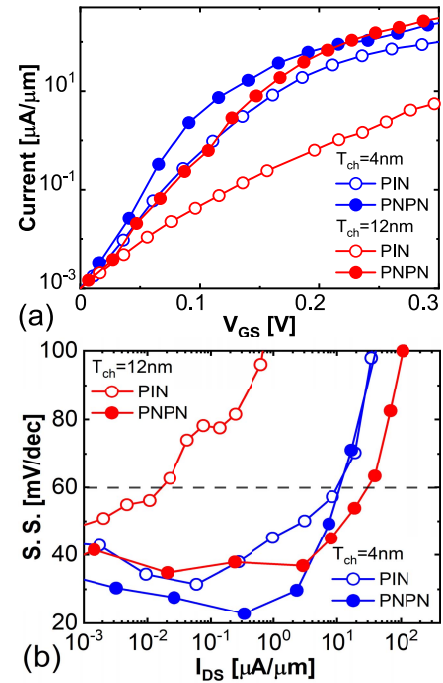


Fig. 3. (a) Transfer I - V characteristics and (b) SS- I_{DS} curve of a THJ TFET with a conventional doping profile (p-i-n) and the optimized doping profile (p-n-p-n) for different body thicknesses (T_{ch}) of 4 and 12 nm.

Fig. 3(a) compares the transfer characteristics of THJ-TFETs with 4- and 12-nm body thicknesses for different doping profiles. The gate-to-source bias (V_{GS}) are shifted to have a fixed OFF-current (I_{OFF}) value of $10^{-3} \mu A/\mu m$ at $V_{GS} = 0$ V. Noted that I_{OFF} is chosen between International Roadmap for Devices and Systems (IRDS) high performance (HP) and low performance's (LP's) spec ($I_{OFF} = 100 \text{ pA}/\mu m$ – $100 \text{ nA}/\mu m$). If a lower I_{OFF} is chosen, the corresponding ON-current (I_{ON}) is lower. For THJ-TFET with the p-i-n doping profile, when the body thickness increases from 4 to 12 nm, the loss of gate control dominates the performance such that I_{ON} decreases by a factor of ~ 16 .

However, for the THJ-TFET with the optimized p-n-p-n doping profile, the same thickness increment is shown to improve the ON-current by $\sim 30\%$. The reason is that, when the body thickness increases from 4 to 12 nm, the engineered built-in electric field in the tunneling junction alleviates the effect of gate control degradation by a better doping profile design. At the same time, the decrease in the confined materials' bandgaps (E_g) enhances the ON-current [27]. The bandgaps of the materials used in the heterojunctions for different body thicknesses are listed in Table I. The ON-current of the THJ-TFET with different body thicknesses and the doping profiles is summarized in Table II.

The SS- I_{DS} curve for the THJ-TFETs with the p-i-n doping profile and the optimized p-n-p-n doping profile for 4- and 12-nm-thick THJ-TFETs are demonstrated in Fig. 3(b). For a body thickness of 4 nm, the SS for the conventional p-i-n doping profile and the optimized p-n-p-n doping profile does not show a significant difference. Both doping profiles exhibit decent performance. However, as the body thickness increases

TABLE I

CONFINED BANDGAP (E_g) AND VALENCE BAND OFF-SET (ΔE_v) OF THE HETEROJUNCTION MATERIALS USED IN THE DESIGN. THE UTB'S CONFINEMENT DIRECTION IS ALONG (110). THE ATOMISTIC TIGHT-BINDING PARAMETERS USED IN THIS WORK ARE FROM [30]

| T_{ch} | | InGaAs | GaAsSb | InAs | GaAsSb |
|----------|-------------------|--------|--------|--------|---------|
| 4 nm | E_g [eV] | 0.9517 | 0.9871 | 0.7016 | 1.504 |
| | ΔE_v [eV] | 0 | 0.4238 | 0.0456 | -0.3796 |
| 12 nm | E_g [eV] | 0.7993 | 0.8456 | 0.5010 | 1.3822 |
| | ΔE_v [eV] | 0 | 0.4273 | 0.0670 | -0.3902 |

TABLE II

ON-CURRENT (I_{ON}) OF THE THJ TFET WITH BODY THICKNESSES OF 4 AND 12 nm FOR BOTH CONVENTIONAL P-I-N DOPING PROFILE AND THE P-N-P-N DOPING PROFILE. THE I_{ON} IS EXTRACTED AT $V_{GS} = 0.3$ V

| T_{ch} | 4 nm | 12 nm | 4 nm | 12nm |
|----------------------------|-------|-------|--------|--------|
| Doping profile | (PIN) | (PIN) | (PNPN) | (PNPN) |
| I_{ON} [$\mu A/\mu m$] | 98 | 6 | 248 | 325 |

to 12 nm, the optimized p-n-p-n doping profile retains its HP, whereas the conventional p-i-n doping profile degrades drastically.

To further understand why THJ-TFET with the optimized p-n-p-n doping profile has a better performance comparing to the case of the traditional p-i-n doping profile, the LDOSs at $V_{GS} = 0.3$ V for different body thicknesses and different doping profiles are shown in Fig. 4.

When the channel thickness of the p-i-n-doped THJ-TFET increases from 4 to 12 nm, the quantum well states are misaligned, as shown in Fig. 4(a) and (c). The resonant states in the InAs channel quantum well are outside the tunneling window. The lack of resonance tunneling leads to significant degradation of the transmission probability and the ON-current. On the other hand, the optimized p-n-p-n doping profile helps to retain the alignment of GaAsSb and InAs quantum well states in the 12-nm-thick THJ-TFET, as shown in Fig. 4(d). The performance of 12-nm-thick THJ-TFETs with the optimized p-n-p-n doping profile is, therefore, similar to the case of a thinner channel thickness.

The tunneling distance is determined by the electric field in TFET's tunneling region. Generally, the tunneling distance of a TFET with a conventional p-i-n doping profile is highly sensitive to the body thickness; a thinner device has a stronger gate control that leads to a smaller natural scaling length and, hence, a smaller tunneling distance [47], [66], [67]. Since the device with an optimized p-n-p-n doping profile has no intrinsic region in the channel, the scaling lengths are dominated by the depletion width corresponding to the doping profile [67]. As a result, the optimized p-n-p-n doping profile is not just engineered to increase the electric field in the tunneling junction; it also reduces the sensitivity of the performance to the body thickness. Fig. 5 shows the impact of doping profile and body thickness on the electric field along the channel. The peak electric field in p-n-p-n-doped

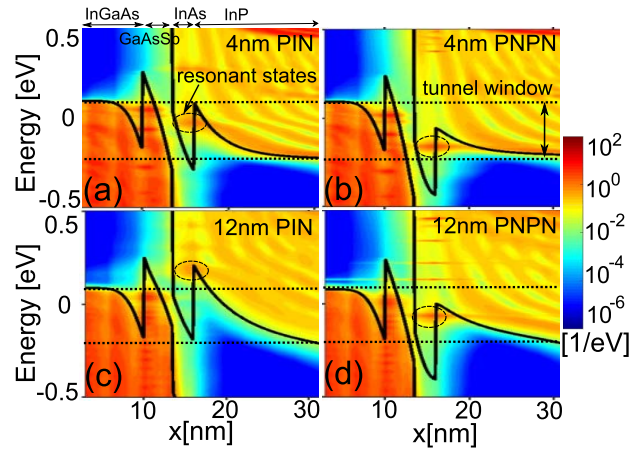


Fig. 4. LDOSs of the THJ TFETs with the body thickness/doping profile of (a) 4 nm/p-i-n, (b) 4 nm/p-n-p-n, (c) 12 nm/p-i-n, and (d) 12 nm/p-n-p-n. LDOS is calculated in the ON-state where $V_{GS} = 0.3$ V.

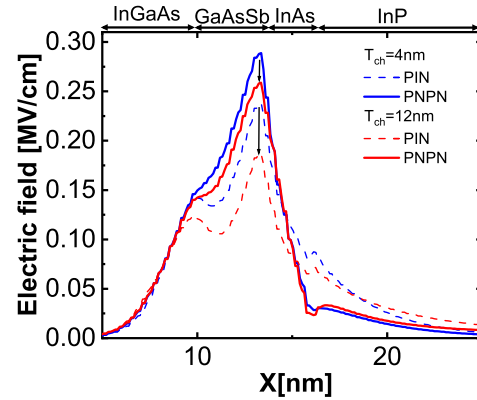


Fig. 5. Electric field along the channel for 4- and 12-nm-thick THJ TFETs with both conventional p-i-n doping profile and optimized p-n-p-n doping profile. The electric field is obtained for the ON-state with $V_{GS} = 0.3$ V.

THJ-TFETs has less dependence on the body thickness compared to the conventional p-i-n-doped THJ-TFETs.

V. P-DOPED INP CHANNEL DOPING DENSITY

The benefit of having a p-n junction in the tunneling region is intuitive and is well-studied [62]–[65]. The electric field in the tunneling region is enhanced by the p-n junction's built-in potential and, therefore, leads to a smaller tunneling distance and a larger transmission probability. The design rule of the p-n junction in the tunneling region is to maximize the doping density to achieve the maximum built-in potential. However, the role of the P-doped channel in the p-n-p-n-doped THJ-TFET is not yet well understood. In this section, the doping density of the P-doped InP channel is studied.

The transfer characteristics and $SS-I_{DS}$ curve of p-n-p-n-doped THJ-TFET with different P-InP channel doping density are shown in Fig. 6. The body thickness of the device is 12 nm. The ON-current at $V_{GS} = 0.3$ V is summarized in Table III. The p-n-p-n-doped THJ-TFET with P-InP channel doping density of $1 \times 10^{16} \text{ cm}^{-3}$ is the reference case to observe the improvement from applying the p-n junction in the tunneling region. The ON-current increases

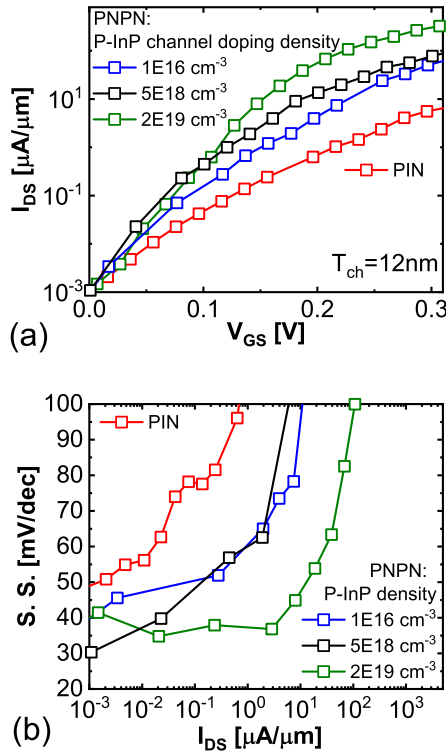


Fig. 6. (a) Transfer I - V characteristics and (b) SS- I_{DS} curve of the 12-nm-thick THJ TFETs with the p-i-n and p-n-p-n doping profile for $V_{DS} = 0.3$ V. The p-n-p-n-doped TFETs with different P-InP channel doping densities are demonstrated.

TABLE III

I_{ON} AT $V_{GS} = 0.3$ V OF THE 12-nm-THICK THJ-TFET WITH DIFFERENT DOPING PROFILES, SUCH AS CONVENTIONAL p-i-n DOPING PROFILE AND THE p-n-p-n DOPING PROFILE

| Doping profile | PIN | PNPN | PNPN | PNPN |
|----------------------------|-----|--------------------|--------------------|--------------------|
| P-InP channel doping | - | 1×10^{16} | 5×10^{18} | 2×10^{19} |
| I_{ON} [$\mu A/\mu m$] | 6 | 50 | 78 | 325 |

from 6 to 50 $\mu A/\mu m$ when the doping profile is replaced from p-i-n doping profile to p-n-p-n doping profile with P-InP channel doping density of $1 \times 10^{16} \text{ cm}^{-3}$.

Interestingly, the performance of 12-nm-thick THJ-TFET improves slightly when P-InP channel doping density increases from 1×10^{16} to $5 \times 10^{18} \text{ cm}^{-3}$. The ON-current increases from 50 to 78 $\mu A/\mu m$. The case with the InP channel doped to $5 \times 10^{18} \text{ cm}^{-3}$ shows sub-40-mV/decade SS for a limited range of drain current (I_{DS}). However, when the P-InP channel doping density further increases to $2 \times 10^{19} \text{ cm}^{-3}$, the performance improves significantly. The ON-current of such case reaches 325 $\mu A/\mu m$. It exhibits the SS less than 40 mV/decade over four orders of magnitude in the drain current.

To further understand the impact of P-InP channel doping density, the ON-state LDOS is compared in Fig. 7. In Fig. 7, the LDOS and the band diagram are extracted at 1 nm away from the edge of the channel, where the potential is strongly affected by the gate bias. The resonant states in InAs quantum well are outside of the tunneling window in the case of p-i-n doping profile. On the other hand, for the cases of

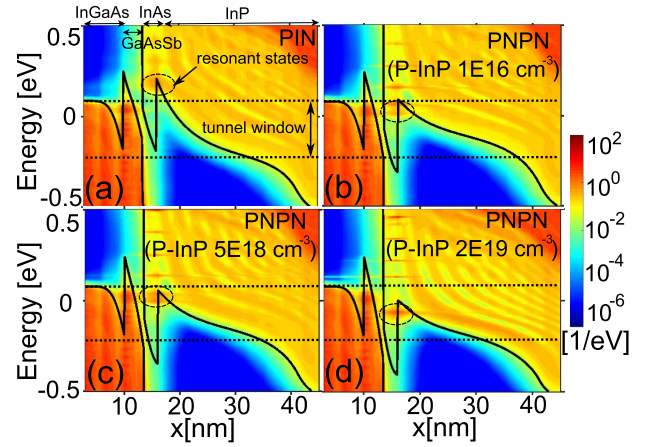


Fig. 7. LDOSs of 12-nm-thick THJ-TFET with (a) p-i-n doping profile and (b)-(d) p-n-p-n doping profile. The P-InP channel doping densities in (b)-(d) are 1×10^{16} , 5×10^{18} , and $2 \times 10^{19} \text{ cm}^{-3}$, respectively. The LDOSs is calculated for the ON-state with $V_{GS} = 0.3$ V.

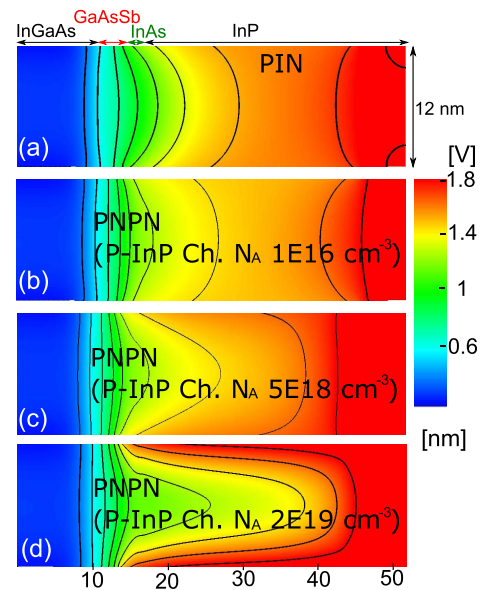


Fig. 8. Channel potential of (a) p-i-n and (b)-(d) p-n-p-n doping profile. The P-InP channel doping densities in (b)-(d) are $1 \times 10^{16} \text{ cm}^{-3}$, $5 \times 10^{18} \text{ cm}^{-3}$, and $2 \times 10^{19} \text{ cm}^{-3}$, respectively. The potentials here are the valence band potential energy divided by $-e$ and are obtained for the ON-state with $V_{GS} = 0.3$ V.

p-n-p-n-doped THJ-TFET, the resonant states are all located inside the tunneling window regardless of different P-InP channel doping densities. This indicates that the improvement when the P-InP channel doped to $2 \times 10^{19} \text{ cm}^{-3}$ comes from other factors other than the alignment of resonant states. The reason is illustrated through the 2-D channel potential and the band diagram, as shown in Figs. 8 and 9.

Fig. 8 shows the 2-D channel potential for different channel doping profiles. In the case when the P-InP channel doped to $2 \times 10^{19} \text{ cm}^{-3}$, the 2-D channel potential is significantly different from the cases with less channel doping density. The device with such high channel doping density is close to operating in the partially depleted regime; thus, a stronger vertical electric field toward the channel-oxide interface is

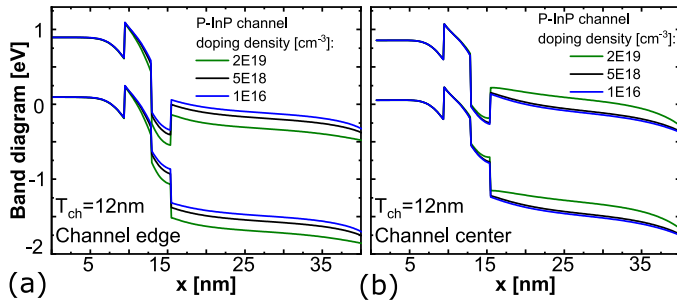


Fig. 9. ON-state band diagram calculated at (a) edge and (b) center of the channel.

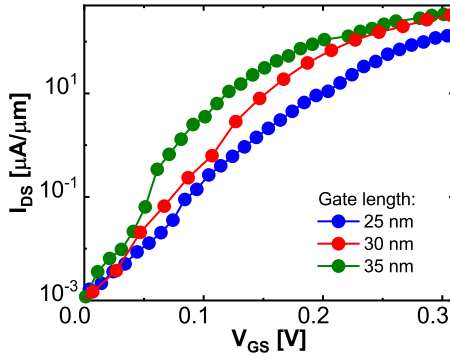


Fig. 10. Transfer I - V characteristic for the optimum design with different gate lengths.

observed. The strong vertical electric field lowers the channel barrier at the channel edge. The triangular potential wells perpendicular to the transport direction are formed at the P-InP channel edge, enhancing the electron confinement at the channel-oxide interface.

Fig. 9(a) and (b) shows the band diagram at the edge and the center of the channel, respectively. As the channel doping density increases to $2 \times 10^{19} \text{ cm}^{-3}$, the conduction band at the channel edge that is close to the channel-oxide interface (depleted region) is pushed down. The reduced channel potential barrier enhances the tunneling current at the channel edge. On the other hand, the channel center's conduction band is pulled up for the heavily P-doped InP channel. This higher channel potential barrier blocks the tunneling current at the channel center, which is weakly controlled by the gate. The surface tunneling current becomes the main contribution to the ON-current. Therefore, the improved electrostatics given by the heavily P-doped channel is the key to the HP for a thick-body TFET.

VI. CONCLUSION

A THJ TFET design is proposed, considering fabrication constraints, such as the channel thickness and the limitation in doping density of the materials. A THJ TFET with a conventional p-i-n doping profile is shown to degrade in performance when the body thickness increases from 4 to 12 nm. The new doping profile is engineered to increase the electric field in the tunneling junction and reduce the sensitivity of the performance to the body thickness. The ON-current of the optimized design reaches $325 \mu\text{A}/\mu\text{m}$, and the SS is less

TABLE IV
 I_{ON} AT $V_{GS} = 0.3 \text{ V}$ OF THE OPTIMUM DESIGN WITH DIFFERENT GATE LENGTHS

| Gate length | 25 nm | 30 nm | 35 nm |
|------------------------------------|-------|-------|-------|
| $I_{ON} [\mu\text{A}/\mu\text{m}]$ | 130 | 325 | 337 |

than 40 mV/decade over four orders of magnitude in the drain current. In this work, 4- and 12-nm body thicknesses are used to demonstrate the doping profile optimization concept. The effect of body thickness variability on TFET's performance, which can be partially mitigated by the p-n-p-n doping profile in principle, requires further study in the future.

APPENDIX: IMPACT OF GATE LENGTH VARIATION

In this work, the proposed design in Fig. 1(b) has a gate length of 30 nm. In this appendix, the transfer I - V characteristics for different gate lengths are shown in Fig. 10. I_{ON} at $V_{GS} = 0.3 \text{ V}$ is listed in Table IV. When the gate length increases from 30 to 35 nm, the ON-current does not increase significantly. As the gate length reduces from 30 to 25 nm, the ON-current reduces to $130 \mu\text{A}/\mu\text{m}$ due to a worse gate control. A detailed analysis on the short-channel effect (such as drain-induced barrier tunneling) requires further study in the future [68], [69].

REFERENCES

- [1] M. Bohr. (2011). *Intel's Revolutionary 22 nm Transistor Technology*. [Online]. Available: http://download.intel.com/newsroom/kits/22nm/pdfs/22nm-Details_Presentation.pdf
- [2] R. Gonzalez, B. M. Gordon, and M. A. Horowitz, "Supply and threshold voltage scaling for low power CMOS," *IEEE J. Solid-State Circuits*, vol. 32, no. 8, pp. 1210–1216, Aug. 1997, doi: 10.1109/4.604077.
- [3] E. Memisevic, J. Svensson, M. Hellenbrand, E. Lind, and L.-E. Wernersson, "Vertical InAs/GaAsSb/GaSb tunneling field-effect transistor on Si with $S = 48 \text{ mV/decade}$ and $I_{on} = 10 \mu\text{A}/\mu\text{m}$ for $I_{off} = 1 \text{ nA}/\mu\text{m}$ at $V_{DS} = 0.3\text{V}$," in *IEDM Tech. Dig.*, Dec. 2016, pp. 9.1.1–19.1.4, doi: 10.1109/iedm.2016.7838450.
- [4] E. Memisevic, J. Svensson, E. Lind, and L.-E. Wernersson, "InAs/InGaAsSb/GaSb nanowire tunnel field-effect transistors," *IEEE Trans. Electron Devices*, vol. 64, no. 11, pp. 4746–4751, Nov. 2017, doi: 10.1109/ted.2017.2750763.
- [5] E. Memisevic, J. Svensson, E. Lind, and L.-E. Wernersson, "Vertical nanowire TFETs with channel diameter down to 10 nm and point SMIN of 35 mV/Decade," *IEEE Electron Device Lett.*, vol. 39, no. 7, pp. 1089–1091, Jul. 2018, doi: 10.1109/led.2018.2836862.
- [6] D. K. Mohata *et al.*, "Demonstration of MOSFET-like on-current performance in arsenide/antimonide tunnel FETs with staggered heterojunctions for 300 mV logic applications," in *IEDM Tech. Dig.*, Dec. 2011, pp. 33.5.1–33.5.4, doi: 10.1109/iedm.2011.6131665.
- [7] S. Sant *et al.*, "Lateral InAs/Si p-type tunnel FETs integrated on Si—Part 2: Simulation study of the impact of interface traps," *IEEE Trans. Electron Devices*, vol. 63, no. 11, pp. 4240–4247, Oct. 2016, doi: 10.1109/TED.2016.2612484.
- [8] J. Appenzeller, Y.-M. Lin, J. Knoch, and P. Avouris, "Band-to-band tunneling in carbon nanotube field-effect transistors," *Phys. Rev. Lett.*, vol. 93, no. 19, Nov. 2004, Art. no. 196805, doi: 10.1103/physrevlett.93.196805.
- [9] J. Appenzeller, Y.-M. Lin, J. Knoch, Z. Chen, and P. Avouris, "Comparing carbon nanotube transistors—The ideal choice: A novel tunneling device design," *IEEE Trans. Electron Devices*, vol. 52, no. 12, pp. 2568–2576, Dec. 2005, doi: 10.1109/ted.2005.859654.
- [10] A. M. Ionescu and H. Riel, "Tunnel field-effect transistors as energy-efficient electronic switches," *Nature*, vol. 479, no. 7373, pp. 329–337, Nov. 2011, doi: 10.1038/nature10679.

- [11] U. E. Avci, D. H. Morris, and I. A. Young, "Tunnel field-effect transistors: Prospects and challenges," *IEEE J. Electron Devices Soc.*, vol. 3, no. 3, pp. 88–95, May 2015, doi: [10.1109/jeds.2015.2390591](https://doi.org/10.1109/jeds.2015.2390591).
- [12] C.-S. Pang *et al.*, "WSe₂ homojunction devices: Electrostatically configurable as diodes, MOSFETs, and tunnel FETs for reconfigurable computing," *Small*, vol. 15, no. 41, Oct. 2019, Art. no. 1902770, doi: [10.1002/smll.201902770](https://doi.org/10.1002/smll.201902770).
- [13] K. Tomioka, M. Yoshimura, and T. Fukui, "Steep-slope tunnel field-effect transistors using III-V nanowire/Si heterojunction," in *Proc. Symp. VLSI Technol. (VLSIT)*, Jun. 2012, pp. 47–48, doi: [10.1109/VLSIT.2012.6242454](https://doi.org/10.1109/VLSIT.2012.6242454).
- [14] D. Cutaia, K. E. Moselund, H. Schmid, M. Borg, A. Olziersky, and H. Riel, "Complementary III-V heterojunction lateral NW tunnel FET technology on Si," in *Proc. IEEE Symp. VLSI Technol.*, Jun. 2016, pp. 1–2, doi: [10.1109/VLSIT.2016.7573444](https://doi.org/10.1109/VLSIT.2016.7573444).
- [15] A. I. Khan, C. W. Yeung, C. Hu, and S. Salahuddin, "Ferroelectric negative capacitance MOSFET: Capacitance tuning antiferroelectric operation," in *IEDM Tech. Dig.*, Dec. 2011, p. 11.3.1–11.3.4, doi: [10.1109/IEDM.2011.6131532](https://doi.org/10.1109/IEDM.2011.6131532).
- [16] K.-S. Li *et al.*, "Sub-60 mV-swing negative-capacitance FinFET without hysteresis," in *IEDM Tech. Dig.*, Dec. 2015, pp. 22.6.1–22.6.4, doi: [10.1109/IEDM.2015.7409760](https://doi.org/10.1109/IEDM.2015.7409760).
- [17] A. C. Seabaugh and Q. Zhang, "Low-voltage tunnel transistors for beyond CMOS logic," *Proc. IEEE*, vol. 98, no. 12, pp. 2095–2110, Dec. 2010, doi: [10.1109/JPROC.2010.2070470](https://doi.org/10.1109/JPROC.2010.2070470).
- [18] T. A. Ameen, H. Ilatikhameneh, P. Fay, A. Seabaugh, R. Rahman, and G. Klimeck, "Alloy engineered nitride tunneling field-effect transistor: A solution for the challenge of heterojunction TFETs," *IEEE Trans. Electron Devices*, vol. 66, no. 1, pp. 736–742, Jan. 2019, doi: [10.1109/ted.2018.2877753](https://doi.org/10.1109/ted.2018.2877753).
- [19] H. Ilatikhameneh, T. A. Ameen, G. Klimeck, J. Appenzeller, and R. Rahman, "Dielectric engineered tunnel field-effect transistor," *IEEE Electron Device Lett.*, vol. 36, no. 10, pp. 1097–1100, Oct. 2015, doi: [10.1109/LED.2015.2474147](https://doi.org/10.1109/LED.2015.2474147).
- [20] U. E. Avci and I. A. Young, "Heterojunction TFET scaling and resonant-TFET for steep subthreshold slope at sub-9 nm gate-length," in *IEDM Tech. Dig.*, Dec. 2013, pp. 4.3.1–4.3.4, doi: [10.1109/IEDM.2013.6724559](https://doi.org/10.1109/IEDM.2013.6724559).
- [21] T. A. Ameen, H. Ilatikhameneh, G. Klimeck, and R. Rahman, "Few-layer phosphorene: An ideal 2D material for tunnel transistors," *Sci. Rep.*, vol. 6, no. 1, pp. 1–7, Sep. 2016, doi: [10.1038/srep28515](https://doi.org/10.1038/srep28515).
- [22] J. Z. Huang, P. Long, M. Povolotskiy, G. Klimeck, and M. J. W. Rodwell, "P-type tunnel FETs with triple heterojunctions," *IEEE J. Electron Devices Soc.*, vol. 4, no. 6, pp. 410–415, Nov. 2016, doi: [10.1109/JEDS.2016.2614915](https://doi.org/10.1109/JEDS.2016.2614915).
- [23] P. Long, J. Z. Huang, M. Povolotskiy, D. Verreck, G. Klimeck, and M. J. W. Rodwell, "High-current InP-based triple heterojunction tunnel transistors," in *Proc. Compound Semiconductor Week (CSW) Includes 28th Int. Conf. Indium Phosph. Rel. Mater. (IPRM) 43rd Int. Symp. Compound Semiconductors (ISCS)*, Jun. 2016, pp. 1–2, doi: [10.1109/ICIPRM.2016.7528592](https://doi.org/10.1109/ICIPRM.2016.7528592).
- [24] P. Long *et al.*, "A high-current InP-channel triple heterojunction tunnel transistor design," in *Proc. 75th Annu. Device Res. Conf. (DRC)*, Jun. 2017, pp. 10–12, doi: [10.1109/DRC.2017.7999437](https://doi.org/10.1109/DRC.2017.7999437).
- [25] Z. J. Huang, P. Long, M. Povolotskiy, G. Klimeck, and J. W. Mark Rodwell, "Sb- and Al-free ultra-high-current tunnel FET designs," in *Proc. 5th Berkeley Symp. Energy Efficient Electron. Syst. Steep Transistors Workshop (ES)*, Oct. 2017, pp. 8–10, doi: [10.1109/E3S.2017.8246174](https://doi.org/10.1109/E3S.2017.8246174).
- [26] H. Ilatikhameneh, T. A. Ameen, C. Chen, G. Klimeck, and R. Rahman, "Sensitivity challenge of steep transistors," *IEEE Trans. Electron Devices*, vol. 65, no. 4, pp. 1633–1639, Apr. 2018, doi: [10.1109/TED.2018.2808040](https://doi.org/10.1109/TED.2018.2808040).
- [27] C.-Y. Chen, T. A. Ameen, H. Ilatikhameneh, R. Rahman, G. Klimeck, and J. Appenzeller, "Channel thickness optimization for ultrathin and 2-D chemically doped TFETs," *IEEE Trans. Electron Devices*, vol. 65, no. 10, pp. 4614–4621, Oct. 2018, doi: [10.1109/TED.2018.2862408](https://doi.org/10.1109/TED.2018.2862408).
- [28] S. Steiger, M. Povolotskiy, H.-H. Park, T. Kubis, and G. Klimeck, "NEMOS: A parallel multiscale nanoelectronics modeling tool," *IEEE Trans. Nanotechnol.*, vol. 10, no. 6, pp. 1464–1474, Nov. 2011, doi: [10.1109/TNANO.2011.2166164](https://doi.org/10.1109/TNANO.2011.2166164).
- [29] J. E. Fonseca *et al.*, "Efficient and realistic device modeling from atomic detail to the nanoscale," *J. Comput. Electron.*, vol. 12, no. 4, pp. 592–600, 2013.
- [30] Y. Tan, M. Povolotskiy, T. Kubis, T. B. Boykin, and G. Klimeck, "Transferable tight-binding model for strained group IV and III-V materials and heterostructures," *Phys. Rev. B, Condens. Matter*, vol. 94, no. 4, pp. 1–17, Jul. 2016, doi: [10.1103/PhysRevB.94.045311](https://doi.org/10.1103/PhysRevB.94.045311).
- [31] M. Luisier and G. Klimeck, "Atomistic full-band simulations of silicon nanowire transistors: Effects of electron-phonon scattering," *Phys. Rev. B, Condens. Matter*, vol. 80, no. 15, pp. 1–11, Oct. 2009, doi: [10.1103/PhysRevB.80.155430](https://doi.org/10.1103/PhysRevB.80.155430).
- [32] R. Lake, G. Klimeck, R. C. Bowen, and D. Jovanovic, "Single and multiband modeling of quantum electron transport through layered semiconductor devices," *J. Appl. Phys.*, vol. 81, no. 12, pp. 7845–7869, Jun. 1997, doi: [10.1063/1.365394](https://doi.org/10.1063/1.365394).
- [33] J. Geng *et al.*, "Quantitative multi-scale, multi-physics quantum transport modeling of GaN-based light emitting diodes," *Phys. Status Solidi A*, vol. 215, no. 9, May 2018, Art. no. 1700662, doi: [10.1002/pssa.201700662](https://doi.org/10.1002/pssa.201700662).
- [34] Y. Hsueh, A. Tankasala, Y. Wang, G. Klimeck, M. Simmons, and R. Rahman, "Phonon induced two-electron relaxation in two donor qubits in silicon," in *Proc. APS Meeting Abstr.*, 2016, pp. 5–8.
- [35] J. Salfi *et al.*, "Valley filtering in spatial maps of coupling between silicon donors and quantum dots," *Phys. Rev. X*, vol. 8, no. 3, Aug. 2018, Art. no. 031049, doi: [10.1103/PhysRevX.8.031049](https://doi.org/10.1103/PhysRevX.8.031049).
- [36] A. Tankasala *et al.*, "Two-electron states of a group-V donor in silicon from atomistic full configuration interactions," *Phys. Rev. B, Condens. Matter*, vol. 97, no. 19, May 2018, Art. no. 195301, doi: [10.1103/PhysRevB.97.195301](https://doi.org/10.1103/PhysRevB.97.195301).
- [37] A. Tankasala, Y. Wang, G. Klimeck, and R. Rahman, "Atomistic configuration interaction simulations of two-electron states of donors in silicon," in *Proc. APS Meeting Abstr.*, 2015, p. A37.011.
- [38] F. Mazzola *et al.*, "The sub-band structure of atomically sharp dopant profiles in silicon," *npj Quantum Mater.*, vol. 5, no. 1, p. 34, Jun. 2020, doi: [10.1038/s41535-020-0237-1](https://doi.org/10.1038/s41535-020-0237-1).
- [39] P. Long *et al.*, "Atomistic modeling trap-assisted tunneling in hole tunnel field effect transistors," *J. Appl. Phys.*, vol. 123, no. 17, May 2018, Art. no. 174504, doi: [10.1063/1.5018737](https://doi.org/10.1063/1.5018737).
- [40] C. D. Bessire, M. T. Björk, H. Schmid, A. Schenk, K. B. Reuter, and H. Riel, "Trap-assisted tunneling in Si-InAs nanowire heterojunction tunnel diodes," *Nano Lett.*, vol. 11, no. 10, pp. 4195–4199, Oct. 2011, doi: [10.1021/nl202103a](https://doi.org/10.1021/nl202103a).
- [41] S. Sant and A. Schenk, "Trap-tolerant device geometry for InAs/Si pTFETs," *IEEE Electron Device Lett.*, vol. 38, no. 10, pp. 1363–1366, Oct. 2017, doi: [10.1109/LED.2017.2740262](https://doi.org/10.1109/LED.2017.2740262).
- [42] M. G. Pala and D. Esseni, "Interface traps in InAs nanowire tunnel-FETs and MOSFETs—Part I: Model description and single trap analysis in tunnel-FETs," *IEEE Trans. Electron Devices*, vol. 60, no. 9, pp. 2795–2801, Sep. 2013, doi: [10.1109/TED.2013.2274196](https://doi.org/10.1109/TED.2013.2274196).
- [43] R. N. Sajjad, W. Chern, J. L. Hoyt, and D. A. Antoniadis, "Trap assisted tunneling and its effect on subthreshold swing of tunnel FETs," *IEEE Trans. Electron Devices*, vol. 63, no. 11, pp. 4380–4387, Nov. 2016, doi: [10.1109/TED.2016.2603468](https://doi.org/10.1109/TED.2016.2603468).
- [44] Q. Smets *et al.*, "Calibration of bulk trap-assisted tunneling and Shockley-Read-Hall currents and impact on InGaAs tunnel-FETs," *IEEE Trans. Electron Devices*, vol. 64, no. 9, pp. 3622–3626, Sep. 2017, doi: [10.1109/TED.2017.2724144](https://doi.org/10.1109/TED.2017.2724144).
- [45] J. Z. Huang *et al.*, "A multiscale modeling of triple-heterojunction tunneling FETs," *IEEE Trans. Electron Devices*, vol. 64, no. 6, pp. 2728–2735, Jun. 2017, doi: [10.1109/TED.2017.2690669](https://doi.org/10.1109/TED.2017.2690669).
- [46] T. A. Ameen, H. Ilatikhameneh, J. Z. Huang, M. Povolotskiy, R. Rahman, and G. Klimeck, "Combination of equilibrium and non-equilibrium carrier statistics into an atomistic quantum transport model for tunneling heterojunctions," *IEEE Trans. Electron Devices*, vol. 64, no. 6, pp. 2512–2518, Jun. 2017, doi: [10.1109/TED.2017.2690626](https://doi.org/10.1109/TED.2017.2690626).
- [47] C.-Y. Chen, H. Ilatikhameneh, J. Z. Huang, G. Klimeck, and M. Povolotskiy, "Impact of body thickness and scattering on III-V triple heterojunction TFET modeled with atomistic mode-space approximation," *IEEE Trans. Electron Devices*, vol. 67, no. 8, pp. 3478–3485, Aug. 2020, doi: [10.1109/TED.2020.3002220](https://doi.org/10.1109/TED.2020.3002220).
- [48] M. Fujimatsu, H. Saito, and Y. Miyamoto, "71 mV/dec of sub-threshold slope in vertical tunnel field-effect transistors with GaAsSb/InGaAs heterostructure," in *Proc. Int. Conf. Indium Phosph. Rel. Mater.*, Aug. 2012, pp. 25–28, doi: [10.1109/iciprm.2012.6403309](https://doi.org/10.1109/iciprm.2012.6403309).
- [49] A. Tabata *et al.*, "Surface InAs/InP quantum wells: Epitaxial growth and characterization," in *Proc. 3rd Int. Conf. Indium Phosph. Rel. Mater.*, Apr. 1991, pp. 496–499, doi: [10.1109/ICIPRM.1991.147421](https://doi.org/10.1109/ICIPRM.1991.147421).

- [50] G. Feng, K. Oe, and M. Yoshimoto, "Temperature dependence of Bi behavior in MBE growth of InGaAs/InP," *J. Cryst. Growth*, vols. 301–302, pp. 121–124, Apr. 2007, doi: [10.1016/j.jcrysgro.2006.11.242](https://doi.org/10.1016/j.jcrysgro.2006.11.242).
- [51] B. Lambert *et al.*, "High reflectivity 1.55 μm (Al) GaAsSb/AlAsSb Bragg reflector lattice matched on InP substrates," *Appl. Phys. Lett.*, vol. 66, no. 4, pp. 442–444, Jan. 1995, doi: [10.1063/1.114050](https://doi.org/10.1063/1.114050).
- [52] J. W. Matthews and A. E. Blakeslee, "Defects in epitaxial multilayers. I. Misfit dislocations," *J. Cryst. Growth*, vol. 27, pp. 118–125, Dec. 1974, doi: [10.1016/0022-0248\(74\)90424-2](https://doi.org/10.1016/0022-0248(74)90424-2).
- [53] T. Akazaki, K. Arai, T. Enoki, and Y. Ishii, "Improved InAlAs/InGaAs HEMT characteristics by inserting an InAs layer into the InGaAs channel," *IEEE Electron Device Lett.*, vol. 13, no. 6, pp. 325–327, Jun. 1992, doi: [10.1109/55.145073](https://doi.org/10.1109/55.145073).
- [54] Y. Omura, A. Mallik, and N. Matsuo, "Impact of a spacer dielectric and a gate overlap/underlap on the device performance of a tunnel field-effect transistor," in *MOS Devices for Low-Voltage and Low-Energy Applications*. Hoboken, NJ, USA: Wiley, 2016, pp. 386–398, doi: [10.1002/9781119107361.ch33](https://doi.org/10.1002/9781119107361.ch33).
- [55] M. D. V. Martino, J. A. Martino, and P. G. D. Agopian, "Drain induced barrier thinning on TFETs with different source/drain engineering," in *Proc. 29th Symp. Microelectron. Technol. Devices (SBMicro)*, Sep. 2014, pp. 1–4, doi: [10.1109/SBMicro.2014.6940092](https://doi.org/10.1109/SBMicro.2014.6940092).
- [56] J. Wu, Y. Fang, B. Markman, H. Tseng, and M. J. W. Rodwell, " $L_g = 30$ nm InAs channel MOSFETs exhibiting $f_{max} = 410$ GHz and $f_t = 357$ GHz," *IEEE Electron Device Lett.*, vol. 39, no. 4, pp. 472–475, Feb. 2018, doi: [10.1109/LED.2018.2803786](https://doi.org/10.1109/LED.2018.2803786).
- [57] Y. Fang, H. Tseng, and M. J. W. Rodwell, " $W_e = 100$ nm InP/InGaAs DHBT with self-aligned MOCVD regrown p-GaAs extrinsic base exhibiting $1\Omega\text{-}\mu\text{m}^2$ base contact resistivity," in *Proc. Device Res. Conf. (DRC)*, Jun. 2019, pp. 179–180, doi: [10.1109/DRC46940.2019.9046400](https://doi.org/10.1109/DRC46940.2019.9046400).
- [58] M.-H. Chiang, J.-N. Lin, K. Kim, and C.-T. Chuang, "Random dopant fluctuation in limited-width FinFET technologies," *IEEE Trans. Electron Devices*, vol. 54, no. 8, pp. 2055–2060, Aug. 2007, doi: [10.1109/TED.2007.901154](https://doi.org/10.1109/TED.2007.901154).
- [59] G. Leung and C. O. Chui, "Variability impact of random dopant fluctuation on nanoscale junctionless FinFETs," *IEEE Electron Device Lett.*, vol. 33, no. 6, pp. 767–769, Jun. 2012, doi: [10.1109/LED.2012.2191931](https://doi.org/10.1109/LED.2012.2191931).
- [60] A. Asenov, "Random dopant induced threshold voltage lowering and fluctuations in sub-0.1 μm MOSFET's: A 3-D 'atomistic' simulation study," *IEEE Trans. Electron Devices*, vol. 45, no. 12, pp. 2505–2513, Dec. 1998, doi: [10.1109/16.735728](https://doi.org/10.1109/16.735728).
- [61] N. Damrongplisit, C. Shin, S. H. Kim, R. A. Vega, and T.-J. King Liu, "Study of random dopant fluctuation effects in germanium-source tunnel FETs," *IEEE Trans. Electron Devices*, vol. 58, no. 10, pp. 3541–3548, Oct. 2011, doi: [10.1109/TED.2011.2161990](https://doi.org/10.1109/TED.2011.2161990).
- [62] V. Nagavarapu, R. Jhaveri, and J. C. S. Woo, "The tunnel source (PNPN) n-MOSFET: A novel high performance transistor," *IEEE Trans. Electron Devices*, vol. 55, no. 4, pp. 1013–1019, Apr. 2008, doi: [10.1109/TED.2008.916711](https://doi.org/10.1109/TED.2008.916711).
- [63] D. B. Abdi and M. J. Kumar, "In-built N^+ pocket p-n-p-n tunnel field-effect transistor," *IEEE Electron Device Lett.*, vol. 35, no. 12, pp. 1170–1172, Dec. 2014, doi: [10.1109/LED.2014.2362926](https://doi.org/10.1109/LED.2014.2362926).
- [64] S. Baronia, K. Nigam, D. Sharma, B. R. Raad, and P. Kondekar, "A novel approach of PNP dual metal double gate tunnel field effect transistor for improving DC characteristics," in *Proc. Int. Conf. Adv. Commun. Control Comput. Technol. (ICACCCT)*, May 2016, pp. 44–47.
- [65] D. B. Abdi and M. J. Kumar, "2-D threshold voltage model for the double-gate p-n-p-n TFET with localized charges," *IEEE Trans. Electron Devices*, vol. 63, no. 9, pp. 3663–3668, Sep. 2016, doi: [10.1109/TED.2016.2589927](https://doi.org/10.1109/TED.2016.2589927).
- [66] H. Ilatikhameneh, G. Klimeck, J. Appenzeller, and R. Rahman, "Scaling theory of electrically doped 2D transistors," *IEEE Electron Device Lett.*, vol. 36, no. 7, pp. 726–728, Jul. 2015, doi: [10.1109/LED.2015.2436356](https://doi.org/10.1109/LED.2015.2436356).
- [67] H. Ilatikhameneh, R. B. Salazar, G. Klimeck, R. Rahman, and J. Appenzeller, "From Fowler–Nordheim to nonequilibrium Green's function modeling of tunneling," *IEEE Trans. Electron Devices*, vol. 63, no. 7, pp. 2871–2878, Jul. 2016, doi: [10.1109/TED.2016.2565582](https://doi.org/10.1109/TED.2016.2565582).
- [68] L. Liu, D. Mohata, and S. Datta, "Scaling length theory of double-gate interband tunnel field-effect transistors," *IEEE Trans. Electron Devices*, vol. 59, no. 4, pp. 902–908, Apr. 2012, doi: [10.1109/TED.2012.2183875](https://doi.org/10.1109/TED.2012.2183875).
- [69] J. Wu, J. Min, and Y. Taur, "Short-channel effects in tunnel FETs," *IEEE Trans. Electron Devices*, vol. 62, no. 9, pp. 3019–3024, Sep. 2015, doi: [10.1109/TED.2015.2458977](https://doi.org/10.1109/TED.2015.2458977).